Co-published by
**Institute of Fluid-Flow Machinery**
Polish Academy of Sciences
**Committee on Thermodynamics and Combustion**
Polish Academy of Sciences



http://www.imp.gda.pl/archives-of-thermodynamics/

# Multiscale entropy applications for complexity analysis of two-phase flow

Gabriela Rafałko[a*], Romuald Mosdorf[a], Hubert Grzybowski[a], Paweł Dzienis[a], Grzegorz Górski[a]

[a]Bialystok University of Technology, Faculty of Mechanical Engineering, Wiejska 45A, Bialystok 15-351, Poland
*Corresponding author email: gabriela.rafalko@pb.edu.pl

Received: 29.12.2023; revised: 15.03.2024; accepted: 20.04.2024

## Abstract

Two-phase flow in channels of small dimensions is often a non-stationary process, the nature of such flow is oscillatory. Due to small channel dimensions, high heat flux, parallel channels interactions, pressure and temperature oscillations, the character of the phenomena occurring during boiling is complex. The changes of the measured signals are observed in different time scales. In order to examine in detail two-phase flow parameters changes, many acquisition devices are often installed. This solution becomes challenging concerning mini and microchannel heat-exchangers due to space limitation and modifications of an experimental setup. This paper presents a novel application of multiscale entropies for spatial and temporal analysis of two-phase flow based on only one registered parameter. This analysis is performed based on pixel brightness changes in photo frames registered by a high speed camera during two-phase flow. The spatial changes of pixel brightness are observed on single frames and temporal changes are examined using a set of frames (in time). The Composite Multiscale Sample Entropy is applied to identify two-phase flow patterns and to analyze the complexity of phase distribution. Using Multivariate Multiscale Sample Entropy the most rapid changes of phase distribution in a multichannel heat exchanger are determined.

**Keywords:** Multiscale entropy; Spatial and temporal image analysis; Two-phase flow; High-speed video

Vol. 45(2024), No. 2, 83–90; doi: 10.24425/ather.2024.150854

Cite this manuscript as: Rafałko, G., Mosdorf, R., Grzybowski, H., Dzienis, P., & Górski, G. (2024). Multiscale entropy applications for complexity analysis of two-phase flow. *Archives of Thermodynamics*, 45(2), 83−90.

## 1. Introduction

The patterns observed during two-phase flow vary in shape, velocity, size and spatial location. The slug flow is characterized with rather long-term changes, on the other hand, during bubbly flow rapid changes occur which are related to bubble location or coalescence. During annular flow the width of a liquid film flowing near the channel wall and liquid droplets in the flow core change in time. Therefore, signals recorded during two-phase flow, such as fluctuations in pressure, temperature, heat flow and changes in the spatial location of pixels recorded during videos, occur in different time scales [1−3]. Non-linear measures, such as multiscale entropies, are used in current papers to study two-phase flow patterns.

In the paper [4], Rescaled Range Permutation Entropy (*RSPE*) was used for analysis of two-phase flow in plexiglass pipe with the diameter of 20 mm based on data collected by conductivity probes. The authors have observed alternations in flow patterns caused abrupt changes in entropy signals. Four typical multivariate multi-scale entropies were applied to exami-

## Nomenclature

$m$ – embedding dimension in *CMSE* algorithm
$M$ – embedding dimension in *MMSE* algorithm
$r$ – distance norm
$q$ – liquid/air flow rate, kg/s

**Greek symbols**

$\varepsilon$ – scale factor
$\tau$ – scale factor in *CMSE* algorithm
$\sigma$ – standard deviation

**Subscripts and Superscripts**

$g$ – gas
$w$ – liquid

**Abbreviations and Acronyms**

*CMSE* – Composite Multiscale Sample Entropy
*MMSE* – Multivariate Multiscale Sample Entropy
*RSPE* – Rescaled Range Permutation Entropy
*MWMPE* – Multivariate Multiscale Weighted Permutation Entropy

ne evolution instability of the data registered with electrical field conductance sensor during oil-water two-phase flow in 20 mm testing pipe [5]. The Multivariate Multiscale Weighted Permutation Entropy (*MWMPE*) presented largest variation range with scale and the best anti-noise ability. The authors of the paper [5] have observed that in the case of very small droplets in the flow, there were weaker fluctuations in sensor signals.

The *CMSE* algorithm has been applied for analysing complex time series including, among others, gait's dynamics [6], river flows [7] or car traffic [8]. A method of analysis for examining the complexity of high-dimensional data within and between individual data series is Multivariate Multiscale Sample Entropy (*MMSE*). This algorithm allows for simultaneous analysis of multi-channel data, enables the examination of linear and non-linear correlations as well as various degrees of synchronization within a given data series and between series [9]. In the paper [2], authors examined horizontal, oil-water two-phase flow data using *MMSE* and concave electrodes. The authors have stated that *MMSE* enables a quantitative analysis of two-phase flow patterns and gives insight into dynamic flow behaviour.

In many of the afore mentioned papers entropy algorithms were applied for spatial (local) analysis of two-phase flow. The installed acquisition devices registered flow parameters only in those parts of the channel where they were placed. In order to gather spatial (local) and temporal changes (in time) of two-phase flow, more acquisition devices have to be mounted. For instance, in the paper [10], authors have observed that an averaged channel surface temperature and critical heat flux were generally insensitive to the flow configurations, thus an additional analysis of two other acquisition parameters (high-frequency pressure, high speed video) was needed. The research direction based on extracting characteristic features from single measurement parameter and using advanced, non-linear tools for its analysis is desirable, especially in the case of industry applications [11].

This paper presents a novel application of multiscale entropy for spatial and temporal analysis of two-phase flow based on only one registered parameter (high speed video). This analysis is performed based on pixel brightness changes in photo frames registered during two-phase flow by a high speed camera. The changes of the pixel brightness in photo frames reflect spatial changes and changes in very short period of time (on the length of the channel). The temporal changes are analysed based on pixel brightness changes in a set of frames. The experimental setup and data characteristics is presented in Section 2. Section 3 shows the application of *CMSE* for flow pattern identification and inlet phenomena complexity analysis. In Section 3 the application of *MMSE* algorithm for identifying the location of the most rapid changes of phase distribution in a multichannel heat exchanger is described. Section 4 presents conclusions.

## 2. Experimental setup and data characteristics

The scheme of the experimental stand is shown in Fig. 1. Two-phase flow of water mixed with glycerol (solution's concentration (weight): 45%) and air was analyzed.

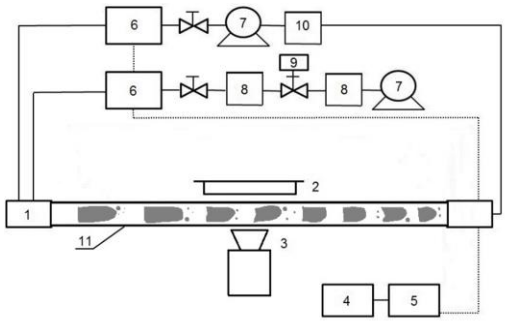


Fig. 1. Scheme of the experimental setup: 1 – minibubbles generator, 2 – light, 3 – high speed camera (Phantom v1610), 4 – PC, 5 – data acquisition station (DT9800, accuracy: 1 mV for voltages od -10V do 10V), 6 – flow meter (Bronkhorst mini CORI-FLOW M13, accuracy ±0,2% flow velocity), 7 – hydraulic pump (Dunkermotoren, BG45x30SI), 8 – air tank, 9 – pressure regulator (Metal Work Regtronic, accuracy: 1 kPa), 10 – liquid tank, 11 – minichannel [12].

The flow through a circular minichannel (11) – see Fig. 1, of a diameter equal to 3 mm and 60 mm long. The rates of water-glycerol and air were constant for each analyzed recording. The special micro-bubbles generator (1) was used to obtain the small bubbles size. The pump (7) generated compressed air which passed through an air tank (8) and a valve (9). Next it was directed to a constant pressure air tank (8), flow meter (6) and special micro – bubbles generator (1). The air rate was controlled by a flow meter (6). The liquid phase was supplied to the tank (10) using the pump (7) and finally heading into minichannel (11). The data acquisition station DT9800 (5) and the PC (4) were connected to the pressure sensors and flow meters. The videos were recorded with a high speed camera with the fre-

quency of 5000 frames per second (3). A light system was installed in the stand (2).

An image analysis of the experimental data was performed based on 56 videos recorded during two-phase flow of water-glycerol and air. The recordings were obtained for a set value of liquid and air flow rates. The flows had a stationary character, their recording began after the system reached a steady state. Bubbles, minibubbles and slugs were observed in the channel.

In Fig. 2 the experimental setup for two-phase flow of distilled water and air was presented. The heat-exchanger with three parallel minichannels was heated using electric power. A vertical row of three thermocouples was installed under minichannels in the copper block (Fig. 2 – $T_1$, $T_2$, $T_3$).

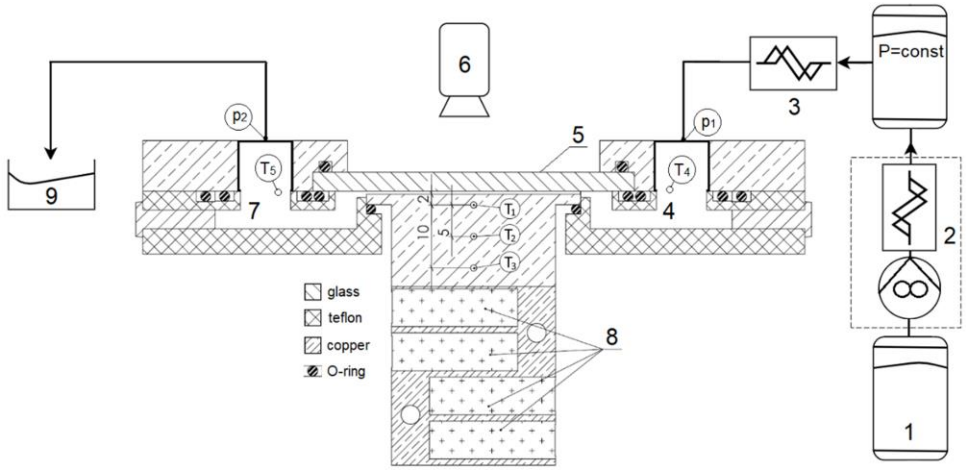


Fig. 2. The experimental setup: 1 – supply tank with distilled water, 2 – gear pump (Tuthill model DGS.11), 3 – compressible volume ($V$ = 222,8 cm$^3$), 4 – flow meter (Bronkhorst mini CORI-FLOW M13, accuracy ± 0,2% of flow velocity), 5 – inlet, 6 – plexiglass, 7 – high speed camera (Phantom v1610), 8 – outlet, 9 – outlet tank, 10 – electric heaters (24V 50 W), $p_1$, $p_2$ – pressure sensors (MPX5050DP, time response: 1 ms), $T_1$, $T_2$, $T_3$, $T_4$, $T_5$ – K-type thermocouples (diameter: 0,081 mm, accuracy: ± 0,8 K, time response: 0,025 s) [13].

The dimensions of minichannels were equal to (width × depth × length) 0.25 × 0.50 × 32 mm (the wall between the channels: 0.25 mm wide). The minichannels were covered with a plexi cover which allowed observations of flow boiling inside minichannels. A high speed camera (7) – see Fig. 2, was used to record flow patterns inside minichannels with the speed of 2000 fps. The working liquid was distilled water. A gear pump (1) pumped the water to the compressible volume tank (2). A Coriolis mass flow meter (3) was used to measure the water mass flow rate. The liquid was flowing into a common inlet area, through three parallel minichannel (5) and headed to an outlet tank (9). The thermocouples ($T_4$, $T_5$) measured temperature in the water inlet and outlet common area. The pressure sensors were used to measure the pressure in inlet and outlet common area ($p_1$, $p_2$). The acquisition systems recorded pressure and temperature signals with a frequency of 1 kHz. The registration of signals and films was synchronized. In this experimental setup two types of multichannel heat-exchanger were examined: 1) three parallel channel system with the following dimensions (width × depth): 0.25 × 0.50 mm, 2) eleven parallel channel system with the following dimensions (width × depth): 0.25 × 0.13 mm. The length of the channels was equal to 34 mm and the wall between channels was 0.25 mm wide. The calculations based on the registered data were peformed in Matlab R2022.

## 3. Multiscale entropy

### 3.1. Composite multiscale entropy

Composite Multiscale Sample Entropy (ang. *CMSE*) allows an analysis of the complexity of data series in different time scales. The first step of this algorithm requires forming a coarse-grained series, ($y_n^{(\tau)}$), from original time series ($x$) [8]:

$$y_{k,n}^{(\tau)} = \frac{1}{\tau}\sum_{i=(n-1)*\tau+k}^{n*\tau+k-1} x_i, \qquad (1)$$

where: $1 \le n \le \frac{N}{\tau}, 1 \le k \le \tau$, $x$ – the original time series, $N$ – the length of each examined time series $x$, $\tau$ – scale factor, $n$ – the length of each coarse-grained time series, $k$ - number of the coarse-grained series for each $\tau$. The length of each coarse-grained time series is equal to $N/\tau$.

When $\tau = 1$, then the coarse-grained series is the original time series. The transformed series, $y_{k,n}^{(\tau)}$, are related to the time scale $\tau$, where the elements of each series are averages of $\tau$ consecutive neighbors in the original time series. The composite procedure takes into account various choices of neighbors (the averaging windows are overlapping). In the coarse-grained time series short-term oscillations are the less noticeable, the higher time scale $t$ is.

The next step of the algorithm is calculating SampEn (Sample Entropy) of each coarse-grained time series. The SampEn is a measure of time series regularity – its high value corresponds to high complexity of an analyzed series [14,15] while its low value corresponds to periodic character of the series.

To calculate SampEn of each new reconstructed signal, $y^{(\tau)}$, following steps are required [8]:

(1) forming $N/(\tau - m + 1)$ vectors:

$$y_m^{(\tau)}(i) = \left[y^{(\tau)}(i), \ldots, y^{(\tau)}(i+m-1)\right], \qquad i = 1, \qquad (2)$$

where $m$ is the length of the compared sequences.

(2) computing the maximum norm:

$$d_m[y_m^{(\tau)}(i), y_m^{(\tau)}(j)] = \max[|\, y_m^{(\tau)}(i+k) - y_m^{(\tau)}(j+k)\,|],\ 0 \le k \le m-1, \quad (3)$$

(3) calculating the sequences with the length $m$ – $B^m{}_i(r)$ and sequences with the length $m+1$ – $A^m{}_i(r)$ which are accepted (within the tolerance $r$):

$$B_i^m(r) = \frac{1}{\frac{N}{\tau}-m+1} c^m(i), \quad i = 1, \dots, \frac{N}{\tau} - m + 1, \quad (4)$$

$$A_i^m(r) = \frac{1}{\frac{N}{\tau}-m+1} c'^{m+1}(i), \quad i = 1, \dots, \frac{N}{\tau} - m + 1, \quad (5)$$

where: $c^m(i)$ is the number of sequences fulfilling the relation $d_m[y_m^{(\tau)}(i), y_m^{(\tau)}(j)] \le r$, $i \ne j$, $c'^{m+1}(i)$ is the number of sequences fulfilling the relation $d_{m+1}[y_{m+1}^{(\tau)}(i), y_{m+1}^{(\tau)}(j)] \le r$, $i \ne j$,

(4) calculating the probability of matching points:

$$B^m(r) = \frac{1}{\frac{N}{\tau}-m+1} \sum_{i=1}^{\frac{N}{\tau}-m+1} B_i^m(r), \quad (6)$$

$$A^m(r) = \frac{1}{\frac{N}{\tau}-m} \sum_{i=1}^{\frac{N}{\tau}-m} A_i^m(r), \quad (7)$$

(5) estimating the sample entropy of data points of finite length:

$$SampEn(m, r, N) = -\ln\left[\frac{A^m(r)}{B^m(r)}\right]. \quad (8)$$

(6) calculating the *CMSE* as the averaged value for $N$ elements in the function of $\tau$:

$$CMSE(x, \tau, m, r) = \frac{1}{\tau}\sum_{n=1}^{\tau} SampEn(y_n^{(\tau)}, m, r) \quad (9)$$

where: $x$ – the original time series, $\tau$ – scale factor, $y_n^{(\tau)}$ – coarse-grained time series with the length of $n$, $m$ – the length of the compared sequences in the coarse-grained time series, $r$ – distance tolerance within compared sequences.

### 3.1.1. Two-phase flow pattern identification

The *CMSE* was applied to identify two-phase flow patterns on each of the 56 registered photo frames (1 frame out of each recorded video) in the experimental stand presented in Fig. 1 [16]. From each frame with the dimensions of 64 × 1280 pixels, the central fragment of a mini-channel with dimensions of 24 × 800 pixels was extracted. Next, the pixel brightness of the extracted region was summed in each column, this way the original time series, $x$, was obtained. Figure 3 shows a video frame and the region of interest marked with a yellow rectangle.

In the next step, coarse-grained time series were calculated according to the Eq. (1). The examples of coarse-grained time series for different photo frames were shown in Fig. 4.

Fig. 3. A photo frame and the analysed area (rectangle) of water-glycerol and air flow: liquid flow rate ($q_w$) and air flow rate ($q_g$): $q_w$ = 43,44 kg/h, $q_g$ = 0,328 l/min [13].

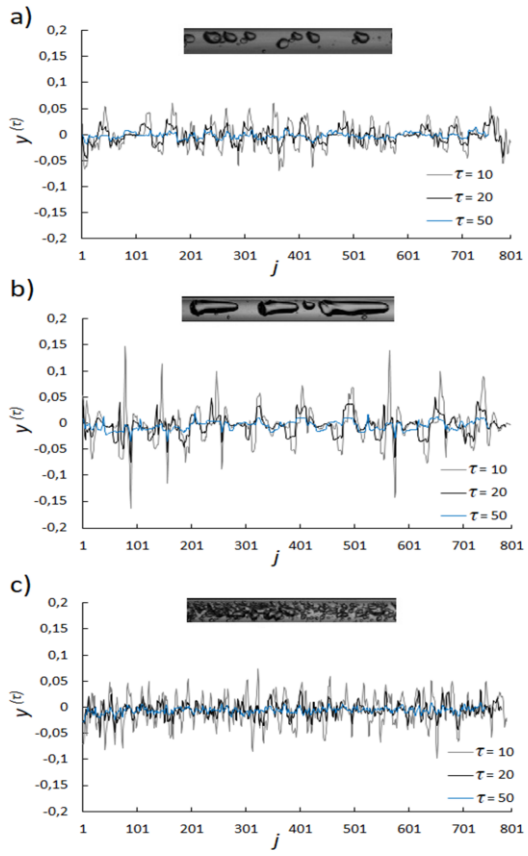


Fig. 4. The coarse-grained time series $y^{(\tau)}$ for $\tau$ = {10,20,50} obtained based on the photo frames presenting: a) bubble flow, b) slug flow, c) minibubble flow (dispersed flow).

The parameters of *CMSE* function were set to the following values: $m$ = 2 – the length of the compared sequences, the standard deviation, $\sigma_\tau$, of each coarse-grained time series was calculated, $r = 0.20*\sigma_\tau$ – the distance tolerance. The *CMSE* functions were calculated. In the last step, the *Complexity Index* (*CI*), which is the integral of *CMSE* function was estimated. The values of the *Complexity Index* for particular data (averaged for 10 subsequent photo frames from one recording) were presented in Table 1.

Table 1. The values of the *Complexity Index* (*CI*) for the analysed *CMSE* functions.

| Two-phase flow pattern | *CI* ± SD | $q_w$ (kg/h) | $q_g$ (l/min) |
|---|---|---|---|
| slugs | 4,24 ± 0,45 | 10,76 | 0,285 |
| | 6,14 ± 0,26 | 16,15 | 0,156 |
| | 7,57 ± 0,07 | 16,15 | 0,242 |
| bubbles and cap bubbles | 10,18 ± 0,07 | 16,15 | 0,070 |
| | 10,48 ± 0,47 | 26,99 | 0,328 |
| | 11,69 ± 0,10 | 32,61 | 0,113 |
| bubbles and minibubbles | 13,36 ± 0,26 | 32,55 | 0,156 |
| | 12,34 ± 0,32 | 21,69 | 0,027 |
| | 13,46 ± 0,36 | 43,54 | 0,070 |
| minibubbles | 15,33 ± 0,13 | 38,15 | 0,070 |
| | 14,60 ± 0,33 | 43,52 | 0,113 |
| | 14,49 ± 0,16 | 38,00 | 0,328 |

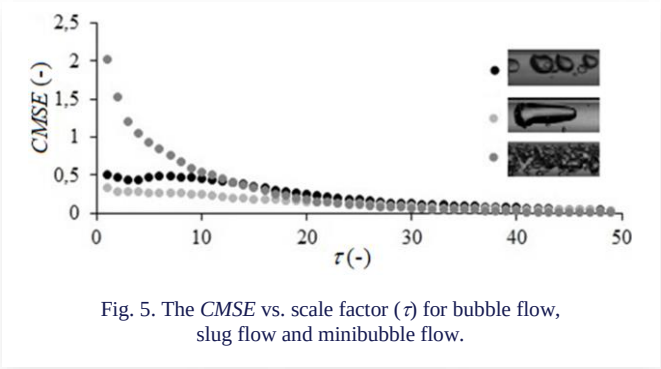


Fig. 5. The *CMSE* vs. scale factor ($\tau$) for bubble flow, slug flow and minibubble flow.

The character of *CMSE* functions for three analysed photo frames was shown in Fig. 5. A hyperbolic shape of *CMSE* is observed for minibubble flow, this data is related to white noise stochastic distribution of small bubbles. For a photo frame representing bubbles, the *CMSE* function has its minimum for $t = 3$, in this case the value of minimum indicates the formation of more correlated (periodic) flow of larger bubbles separated by liquid phase. For a slug flow, more flat distribution of *CMSE* functions is observed informing about the presence of flow correlations but absence of characteristic distance between analysed pixel brightness time series.

### 3.1.2. Inlet flow complexity analysis

The CMSE algorithm was applied to analyze the complexity of pixel brightness changes in photo frames in time recorded with the speed of 2000 fps by a high speed camera. The time between subsequent photo frames corresponded to a formation of a vapour bubble. The length of the time series was equal to 10 s (20 000 data points). An example photo frame and the region of interest ($S_{in}$) in the common inlet of three minichannels were marked in Fig. 6.


Fig. 6. A photo frame of flow boiling in three parallel minichannels; the region of analysis was marked with a rectangle.

The analysed time series of pixel brightness sums were extracted from photo frames with following dimensions: 1.1 × 1.4 mm. The example three times series for two-phase flow recorded at following mass flow rates: 210 g/h, 383 g/h and 570 g/h were shown in Fig. 7.

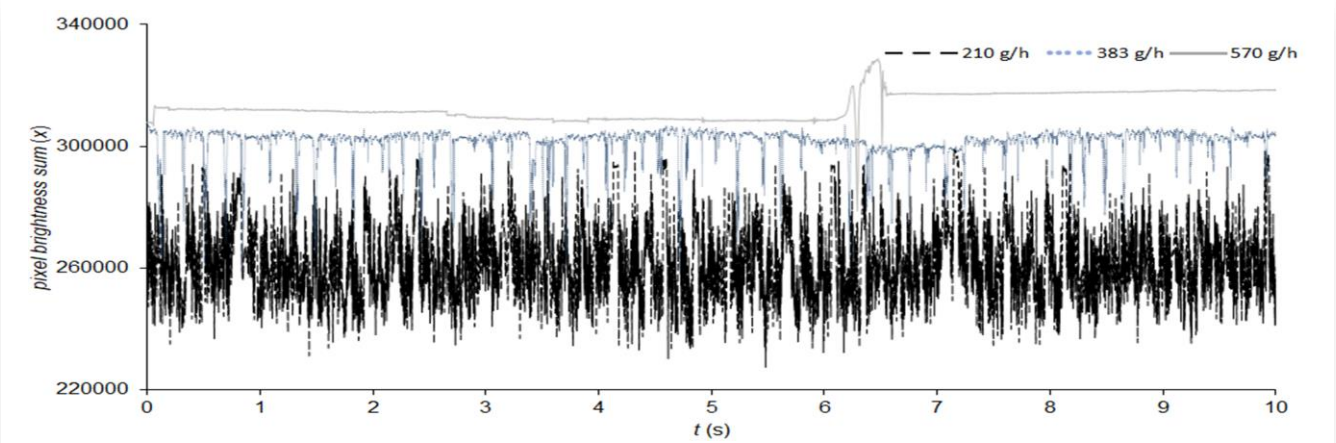


Fig. 7. The sums of pixel brightness in the inlet common area calculated from photo frames recorded during flow boiling for three mass flow rates: 210 g/h, 383 g/h, 570 g/h.

The calculated *CMSE* functions based on the pixel brightness sums in photo frames presenting common inlet of three parallel minichannels were shown in Fig. 8. A hyperbolic-like shape of *CMSE* functions was observed for data registered during flow boiling at lower mass flow rates (175−246 g/h), this corresponds to a stochastic character of phase distribution in the common inlet.

Based on the analyses performed for this experimental data in another paper [17] a high complexity of the inlet flows is related to very intense boiling process, reverse flow, high heat flux, unsynchronized work of minichannels and stochastic changes of pixel brightness. A rather flat distribution of *CMSE* functions was observed for flows with higher water flow rate which informs about a less complex character of pixel brightness changes in the common inlet.

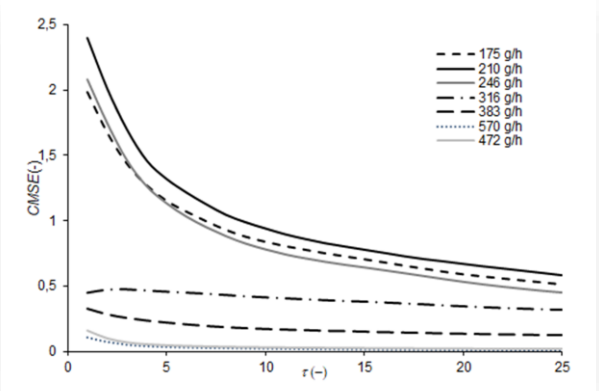


Fig. 8. The CMSE for analysed flows in the function of time scales ($\tau$).

### 3.2. Multiscale multivariate sample entropy

Multivariate Multiscale Sample Entropy, *MMSE*, is used to simultaneously study the complexity of many series, for example to analyze wind velocities from different directions, car traffic on several streets. This algorithm enables the examination of linear and non-linear correlations as well as degrees of synchronization within and between data series. The algorithm takes into account the number of channels (variables) from which the time series comes. The first step is to construct a multivariate coarse-grained time series according to the following formula [8]:

$$y_{k,n}^{(\tau)} = \frac{1}{\tau}\sum_{i=(n-1)*\tau+1}^{n*\tau} x_{k,i}, \tag{10}$$

where: $k = 1,2, \ldots, p$, $1 \le k \le p$, $1 \le i \le N$, $1 \le n \le N/\tau$.

The following steps of the *MMSE* algorithm were presented in Fig. 9 [8]: constructing coarse-grained time series, forming composite delay vectors, defining the maximum distance norm and calculating MSample Entropy.

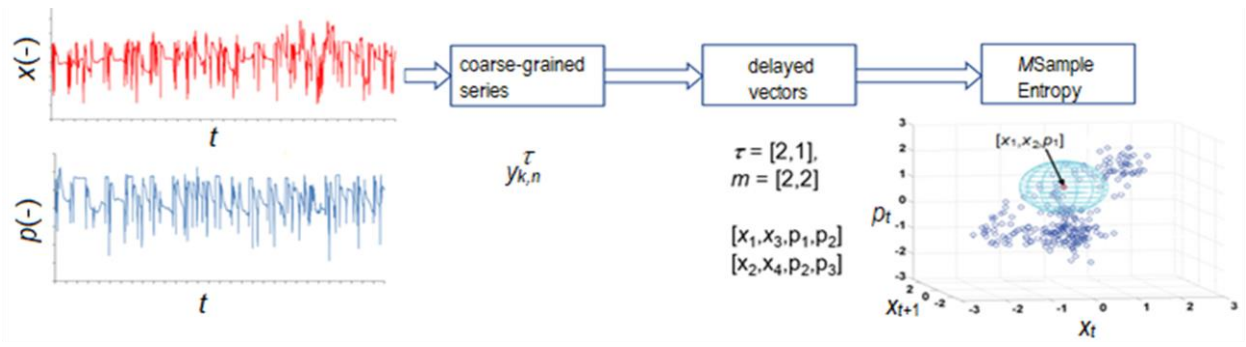


Fig. 9. The steps of *MMSE* algorithm.

#### 3.2.1. Phase distribution complexity analysis

During boiling in mini and micro channels, the rate of the phase distribution changes varies depending on the distance from the inlet, the occurring flow pattern, the delivered heat and mass rate. An analysis of the dynamics of phase distribution changes makes it possible to determine the areas with the most rapid changes. In order to increase the heat dissipation surface, multi-channel systems are used. In this case, separate analyses for each channel are often conducted [18,19]. Such analyses do not take into account interactions between channels in multi-channel heat exchangers which role increases in heat-exchangers with small dimensions channel.

The *MMSE* algorithm described in the section 3.2 was applied to analyse the complexity of the phase distribution in eleven parallel microchannels based on the data registered during flow boiling. Two-phase flow in microchannels was registered with the speed of 3000 fps, the length of each time series was equal to 0.5s (3000 data points), 12 time series were analyzed. The time between subsequent frames (0.0002 s) corresponded to a growth of very small bubble into a bubble with a diameter equal to the channel's width. The analysis of pixel brightness in the photo frames presenting two-phase flow was carried out in the distance ranging from 0 to 660 pixels (from 0 mm to 16.5 mm) from the inlet to the microchannels, as it was shown in Fig. 10.

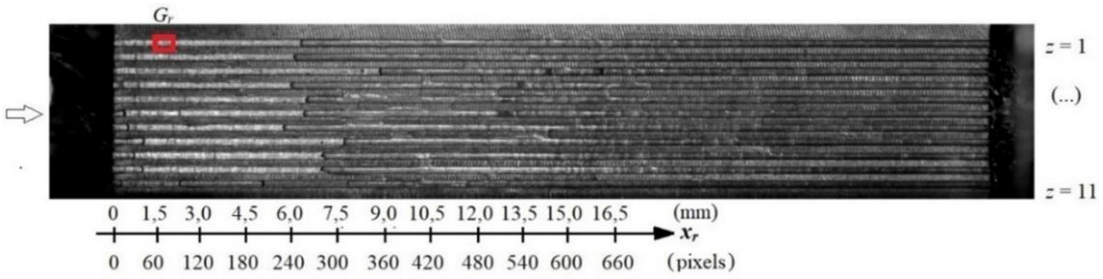


Fig. 10. The example photo frame of flow boiling in eleven parallel microchannels: $z$ – microchannel number, $x_r$ – the locations of the gate $G_r$ (rectangle); the arrow indicates flow's direction [13].

Figure 10 shows the common inlet (on the left) and outlet of the exchanger (on the right) and parallel microchannels ($z$) with the following dimensions (depth × width × length): 0.13 × 0.25 × 32 mm. Below the figure, the $X$-axis is placed, marking the considered positions of the region of interest called the gate, $G_r$, shifted every 1.5 mm (i.e. 60 pixels). The gate's length ($L$ = 20 pixels) corresponded to the length of a short slug or to a pair of bubbles. The brightness of pixels in the image in the case of water flow was higher than in the case of air flow (Fig. 10).

The *MMSE* algorithm was conducted on the data sets containing sums of pixels brightness in gates $G_r$ in each of its positions in time, simultaneously in eleven microchannels. This way the input data matrix had following dimensions: pixel brightness in the gate's location x time x channel number. In the analysis, five scale factors ($\varepsilon$) were considered. The algorithm was calcul-

ated based on the data for subsequent locations of the gate separately. The result of one run of the algorithm is shown in Fig. 11.

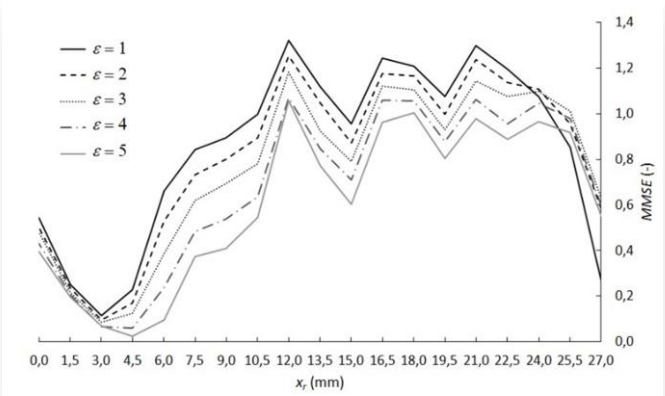


Fig. 11. The *MMSE* vs. position of the gate ($x_r$) for time scales ($\varepsilon$) [13].

As one can notice, the *MMSE* functions reach their maximum for one, particular position of the gate – in this case in the distance of 12 mm from the inlet. Based on the recorded videos and changes in *MMSE* function, it can be concluded that the maximum value of *MMSE* indicates the position in the heat exchanger where the most rapid changes of phase distribution occur. Based on the analyses presented in the paper [13], the location of the most rapid changes of phase distribution is related to a point from which water and air are heading only to the outlet of the exchanger. Between the inlet and the mentioned point, boiling front movement is continuously observed.

In order to verify the repeatability of the algorithm, the calculations were performed for three sets of parameters (1: $M = \{3,1\}$, $\tau = \{1\}$, $r = \{0.05\ \sigma_\tau\}$; 2: $M = \{2\}$, $\tau = \{2,3\}$, $r = \{0.05\ \sigma_\tau\}$; 3: $M = \{2\}$, $\tau = \{1\}$, $r = \{0.03\ \sigma_\tau, 0.07\ \sigma_\tau\}$) and scale factors $\varepsilon = \{1,2,3\}$. In all the runs of the algorithm, the maximum of the *MMSE* was obtained for $x_r = 12.0$ mm which underlines the high applicability of the algorithm regardless of slight changes in the input parameters. This point indicates the maximum position of the boiling front in the heat exchanger.

## 4. Results

In the paper, the *CMSE* algorithm enabled the identification of four different two-phase flow patterns based on high speed photo frames of water-glycerol and air two-phase flow in a minichannel. The *CMSE* algorithm was also used to analyze the complexity of inlet flow during flow boiling in three, parallel minichannels. The level of complexity identified using the *CMSE* algorithm is related to the intensity of boiling process, the synchronization/lack of synchronization between processes in minichannels and the character of changes of pixel brightness in photo frames.

The *MMSE* algorithm was applied for identifying the location of the most rapid changes of phase distribution simultaneously in 11 parallel microchannels. The location of the most rapid changes of phase distribution determines the area of the heat-exchanger where boiling front is continuously moving and heat transfer is the highest. Despite slight changes in parameters of *MMSE* algorithms, the determined location of the most rapid changes of phase distribution was the same. This proves a high applicability of the proposed algorithm.

## 5. Conclusions

This current work presents novel application of multiscale entropies for spatial and temporal analysis of two-phase flow based on one measurement parameter (high speed videos). In the paper, spatial (on a single photo frame) and temporal changes (in a set of subsequent frames) of pixel brightness were analyzed. In the cases under consideration, the sampling frequency of high speed video frames was high enough to later extract characteristic features of two-phase flow based on only one measurement parameter.

It has been shown that multiscale entropies algorithms combined with preliminary analysis of measurement data form an effective tool for identifying two-phase flow patterns and studying their complexity and dynamics. The presented, novel approach to two-phase flow analysis based on only one registered parameter is in an agreement with current research directions, concerning especially industry applications possibilities. The methodology of this paper can be applied, for instance, in dynamical monitoring of oilfields/two-phase flow in small channels due to the non-invasive acquisition method (high speed videos) and the possibilities of complexity and dynamics analyses using multiscale entropies.

## Acknowledgement

The research was funded by the National Science Center grant UMO-2017/27/B/ST8/02905.

## References

[1] Fabila-Carrasco, J.S., Tan, C., & Escudero, J. (2022). *A noise-robust Multivariate Multiscale Permutation Entropy for two-phase flow characterisation*. The University of Edinburgh. Edinburg Research Explorer. doi: 10.48550/arxiv.2210.09030

[2] Gao, Z.-K., Ding, M.-S., Geng, H., & Jin, N.-D. (2015). Multivariate multiscale entropy analysis of horizontal oil–water two-phase flow. *Physica A*, 417, 7–17. doi: 10.1016/j.physa.2014.09.017

[3] Górski, G., Litak, G., Mosdorf, R., & Rysak, A. (2019). Periodic Trends in Two-Phase Flow Through a Vertical Minichannel: Wavelet and Multiscale Entropy Analyses Based on Digital Camera Data. *Acta Mechanica et Automatica*, 13(1), 51–56. doi: 10.2478/ama-2019-0008

[4] Ren, W., Zhang, J., & Jin, N. (2021). Rescaled range permutation entropy: A method for quantifying the dynamical complexity of gas–liquid two-phase slug flow. *Nonlinear Dynamics*, 104(4), 4035–4043. doi: 10.1007/s11071-021-06468-2

[5] Han, Y.-F., Jin, N.-D., Zhai, L.-S., Ren, Y.-Y., & He, Y.-S. (2019). An investigation of oil–water two-phase flow instability using multivariate multi-scale weighted permutation entropy. *Physica A: Statistical Mechanics and Its Applications*, 518, 131–144. doi: 10.1016/j.physa.2018.11.053

[6] Costa, M., Peng, C.-K., L. Goldberger, A., & Hausdorff, J.M. (2003). Multiscale entropy analysis of human gait dynamics.

*Physica A: Statistical Mechanics and Its Applications*, 330(1), 53–60. doi: 10.1016/j.physa.2003.08.022

[7] Li, Z., & Zhang, Y.-K. (2008). Multi-scale entropy analysis of Mississippi River flow. *Stochastic Environmental Research and Risk Assessment*, 22(4), 507–512. doi: 10.1007/s00477-007-0161-y

[8] Zhang, N., Lin, A., Ma, H., Shang, P., & Yang, P. (2018). Weighted multivariate composite multiscale sample entropy analysis for the complexity of nonlinear times series. *Physica A: Statistical Mechanics and Its Applications*, 508, 595–607. doi: 10.1016/ j.physa. 2018.05.085

[9] Ahmed, M.U., & Mandic, D.P. (2012). Multivariate Multiscale Entropy Analysis. *IEEE Signal Processing Letters*, 19(2), 91–94. doi: 10.1109/LSP.2011.2180713

[10] Clark, M.D., Weibel, J.A., & Garimella, S.V. (2023). Impact of pressure drop oscillations and parallel channel instabilities on microchannel flow boiling and critical heat flux. *International Journal of Multiphase Flow*, 161, 104380. doi: 10.1016/j.ijmultiphaseflow.2023.104380

[11] Zhu, L., Jhia Ooi, Z., Zhang, T., Brooks, C.S., & Pan, L. (2023). Identification of flow regimes in boiling flow with clustering algorithms: An interpretable machine-learning perspective. *Applied Thermal Engineering*, 228, 120493. doi: 10.1016/j.applthermaleng.2023.120493

[12] Rafałko, G., Mosdorf, R., & Górski, G. (2020). Two-phase flow pattern identification in minichannels using image correlation analysis. *International Communications in Heat and Mass Transfer*, 113,104508. doi: 10.1016/j.icheatmasstransfer.2020.104508

[13] Rafałko, G.S. (2023). *Application of image analysis to identify and investigate the dynamics of two-phase flow patterns*: PhD thesis, Bialystok University of Technology. https://biblioteka.pb.edu.pl/spisy/2023/206140.djvu [accessed 09 Feb. 2024].

[14] Costa, M., Goldberger, A.L., & Peng, C.K. (2005). Multiscale entropy analysis of biological signals. *Physical Review E*, 71(2), 021906. doi: 10.1103/PhysRevE.71.021906

[15] Richman, J.S., & Moorman, J.R. (2000). Physiological time-series analysis using approximate entropy and sample entropy. *American Journal of Physiology-Heart and Circulatory Physiology*, 278(6), H2039–H2049. doi: 10.1152/ajpheart.2000.278.6.H2039

[16] Rafałko, G., Mosdorf, R., Litak, G., & Górski, G. (2020). Complexity of phase distribution in two-phase flow using composite multiscale entropy. *European Physical Journal Plus*, 135(8). doi: 10.1140/epjp/s13360-020-00686-0

[17] Rafałko, G., Grzybowski, H., Dzienis, P., Mosdorf, R., & Adamowicz, A. (2021). Image Analysis of Flow Maldistribution during Boiling in Parallel Minichannels. *Chemical Engineering and Technology*,44(11), 1978–1985. doi: 10.1002/ceat.202100246

[18] Dario, E.R., Tadrist, L., & Passos, J.C. (2013). Review on two-phase flow distribution in parallel channels with macro and micro hydraulic diameters: Main results, analyses, trends. *Applied Thermal Engineering*, 59(1), 316–335. doi: 10.1016/j.applthermaleng.2013.04.060

[19] Ha, M.Y., Kim, C.H., Jung, Y.W., & Heo, S.G. (2006). Two-Phase Flow Analysis in Multi-Channel. *Journal of Mechanical Science and Technology*, 20(6), 840–848. doi: 10.1007/ BF02915947